PHOTONICS Research

Photonic engineering of superbroadband near-infrared emission in nanoglass composites containing hybrid metal and dielectric nanocrystals

Zhigang Gao,[1,2] Haibo Zhu,[1] Bochao Sun,[1] Yingke Ji,[1] Xiaosong Lu,[1] Hao Tian,[1] Jing Ren,[1,6] Shu Guo,[3] Jianzhong Zhang,[1,7] Jun Yang,[1,4,8] Xiangeng Meng,[5] and Katsuhisa Tanaka[2]

[1]Key Laboratory of In-fiber Integrated Optics, Ministry of Education, Harbin Engineering University, Harbin 150001, China
[2]Department of Material Chemistry, Graduate School of Engineering, Kyoto University, Nishikyo-ku, Kyoto 615-8510, Japan
[3]Center of Analysis and Measurement, Harbin Institute of Technology, Harbin 150001, China
[4]School of Information Engineering, Guangdong University of Technology, Guangzhou 510008, China
[5]Key Laboratory of Processing and Testing Technology of Glass & Functional Ceramics of Shandong Province, School of Materials Science & Engineering, Qilu University of Technology (Shandong Academy of Sciences), Jinan 250353, China
[6]e-mail: ren.jing@hrbeu.edu.cn
[7]e-mail: zhangjianzhong@hrbeu.edu.cn
[8]e-mail: yangj@gdut.edu.cn

Received 3 October 2019; revised 9 February 2020; accepted 6 March 2020; posted 6 March 2020 (Doc. ID 379662); published 24 April 2020

Photonic media containing hybrid noble metal–dielectric nanocrystals (NCs) represent a wonderland of nanophotonics, with a myriad of uncharted optical functions yet to be explored. Capitalizing on the unique phase separation and spontaneous formation of Au-metal NCs in a gallosilicate glass, we fabricated Ni^{2+}-doped transparent nanoglass composites (GCs) containing Au-metal/γ-Ga_2O_3-dielectric NCs. Compared with GCs free of Au-metal NCs, the superbroadband near-infrared emission of Ni^{2+} with a full width at half-maximum over 280 nm is enhanced twice in the Au-metal/γ-Ga_2O_3 dual-phase GCs. A comparison is given as to the spontaneous emission (SPE) properties of Ni^{2+} in the dual-phase GCs when pumped resonantly and off-resonantly with the localized surface plasmon resonance band of the Au-metal NCs. The important role of the Au-metal NCs in the SPE enhancement is revealed by theoretical simulation based on the finite-element method. Combining the photonic engineering effect of hybrid Au-metal/γ-Ga_2O_3 NCs and the sensitization effect of Yb^{3+} on Ni^{2+}, a record-high enhancement factor of over 10 of the Ni^{2+} NIR emission is achieved, and optical gain is demonstrated in the GCs at the fiber communication wavelength.

https://doi.org/10.1364/PRJ.379662

1. INTRODUCTION

Exploiting the advantages of both noble metal (e.g., Au, Ag) and dielectric (e.g., Ga_2O_3, TiO_2) nanocrystals (NCs) for manipulation of light–matter interaction at the subwavelength scale has led to a number of unprecedented technologies to break down the conservative ideas in nanophotonics such as ultracompact light sources [1], ultrahigh density optical data storage [2], ultrasensitive spectroscopy [3], efficient LED lighting [4], and enhanced solar energy harvesting [5]. The light–matter interactions in general and spontaneous emissions (SPEs) in particular are subject to the local photonic environment [6]. For example, modifying local electromagnetic (EM) field enhancements and density of optical states (LDOS), also known as photonic engineering [7], has led to more than 3 orders of magnitude enhancement of upconversion luminescence (UCL) of rare-earth (RE) ion-doped inorganic NCs [8]. On one hand, the enhancement of SPE arises from the strong coupling between emitters and localized surface plasmon resonance (LSPR) of the metal–dielectric NCs [9]. On the other hand, the near-field scattering, due to the presence of a refractive index contrast between the NCs and the surrounding media, may promote utilization of pump light and thus lead to the enhanced SPE [10].

However, it still remains a fundamental challenge to build advanced and robust bulk photonic devices based on metal–dielectric NCs [11]. Previously, implantation of noble metal NCs into bulk photonic glasses has proven to be instrumental in achieving diverse functionalities such as random lasing [12], superior nonlinear optical properties [13], ultrastable optical data memory [14], volumetric Bragg gratings [15], and

surface-enhanced Raman scattering [16]. Recently, glasses embedded with dielectric NCs such as Ga_2O_3 are gaining increasing research momentum, which is continuously driven by their potential applications in solar-blind converters [17] and, when doped with RE or transition metal (TM) ions (e.g., Cr^{3+}, Ni^{2+}), in solid-state lighting and broadband fiber amplifiers [18,19]. Naturally, an interesting question emerges as to what extent the embedded metal-Ga_2O_3 NCs will influence optical and particularly SPE properties of RE or TM ion-doped photonic glasses, which has not been reported in the literature. Essentially, the difficulty lies in the controlled synthesis of nanoglass composites (GCs), also known as nanoglass ceramics, containing the desired metal–dielectric dual-phase NCs and not suffering from serious optical properties degradation as well as other adverse side effects related to microscopic inhomogeneities [20,21].

Capitalizing on the unique phase separation and spontaneous formation of Au-metal NCs in a supercooled gallosilicate glass [22], we fabricated Ni^{2+}-doped transparent GCs containing Au-metal/γ-Ga_2O_3 NCs via a simple one-step thermal-induced crystallization process. The reason for selecting Ni^{2+} as the dopant is primarily its attractive ultrabroadband near-infrared (NIR) SPE covering the second "biological window" (1000–1350 nm) and the important "fiber communication window" (1100–1700 nm). Although significant progress has been made lately to boost Ni^{2+} NIR SPE in GCs, for example, using sensitizers (e.g., Nd^{3+}, Yb^{3+}) to facilitate energy-harvesting of excitation light, new techniques and strategies are still in great demand to meet the insatiable desire for performance improvement. Compared with RE ions, the SPE of TM ions (Ni^{2+}) is much more susceptible to local EM field environments. As such, notable modification of Ni^{2+} SPE is expected to occur in the nanostructured GCs containing the dual-phase metal–dielectric NCs, and consequently observed in our experimental work. The underlying mechanism responsible for the enhanced SPE is discussed in the context of both experimental observations and theoretical simulations.

2. EXPERIMENT

Glass samples with the composition of (in mol.%) $64SiO_2 - 23Ga_2O_3 - 13Li_2O$ doped with 0.15Ni and xAu ($x = 0$, 0.3, 0.5, and 0.7), were prepared by the conventional melt-quenching method. High purity (4N) SiO_2, Ga_2O_3, Li_2O, NiO, and $HAuCl_4 \cdot 3H_2O$ (3N) were used as the raw materials. A total of 30 g raw materials was mixed completely and melted in a high-purity quartz (3N) crucible at 1600°C for 1 h in air. The melt was rapidly quenched at room temperature (RT) and then annealed at 550°C for 3 h, forming "precursor glass" (PG). The PGs were cut and well polished to 12 mm × 10 mm × 1.2 mm cuboids. Finally, GCs were obtained by heating the PGs at 740°C for 5 h. The fabrication details can be found in the Appendix A.

Detailed characterizations include transmission electron microscopy (TEM), high-angle-annular-dark-field scanning TEM (HAADF-STEM), energy dispersive spectroscopy (STEM-EDS), X-ray diffraction (XRD), optical transmission, and steady-state and time-resolved photoluminescence (PL); please refer to the Appendix A. The refractive index, n, was measured by an Abbe refractometer (ATAGO) with a sodium vapor lamp that emits at 589.3 nm (D line). The simulation of the local EM field in the GCs was carried out by a finite-element method using commercially available COMSOL Multiphysics (COMSOL Inc.) software [23]. The wave-optics module was used because it is very suitable for theoretically simulating and analyzing nanostructured optics [24,25]. In the simulation, the outer boundary of the domain was implemented with perfectly matched layers to prevent backreflections.

3. RESULTS AND DISCUSSION

The precursor gallosilicate glass (AuNi PG) is completely amorphous, with no diffraction peaks, as shown in Fig. 1(a). However, an additional weak and broad shoulder is clearly resolved at around $2\theta = 36.2°$ (highlighted by a circle), coinciding with the strongest diffraction peak of the standard γ-Ga_2O_3 spinel, suggesting the occurrence of an submicrometer two-phase structure, similar to our previous work [18]. Owing to the unique phase separation of the supercooled PG, γ-Ga_2O_3 NCs can be grown in the glass matrix upon thermal treatment without the aid of typical heterogeneous nucleating agents such as TiO_2, ZrO_2, CaF_2, Cr_2O_3, and noble metals. However, no diffraction peaks of metallic Au are detected, which might be due to the small size and dilute distribution of Au NCs [26]. The presence of Au NCs, however, can be observed by TEM, as shown in Figs. 1(b)–1(e). Two types of NCs are identified with different morphologies and particle size distributions in the GC, namely, (1) cubic nanoparticles with a larger size (~10 nm, green squares) representing the Ga_2O_3 NCs, and (2) spherical ones with a smaller particle size (~5 nm, blue circles) corresponding to the Au-metal NCs (confirmed by STEM-EDS). The inset in Fig. 1(b) shows the corresponding high-resolution TEM (HRTEM) image, which also evidences the existence of dual-phase NCs as distinguished by the differences in the crystal lattice constants (interplanar spacings). The presence of Au NCs can be further verified by the elemental mapping, as shown in Fig. 1(d). The separation distance between Au-metal and Ga_2O_3 NCs is less than 5 nm (in close proximity), with a considerable faction of Au-metal NCs in contact with Ga_2O_3 NCs. The coupling between Au and Ga_2O_3 NCs within the shaped region, as indicated by a rectangle in Fig. 1(b), will be simulated, as discussed in Fig. 4 later.

The cogrowth of Au/Ga_2O_3 NCs in the GCs imposes spectacular influence on their optical properties. Figure 2 shows transmission spectra of Ni^{2+} singly-doped and Ni^{2+}/Au-codoped PG and GC samples. Similar to our previous studies, the absorption bands at 435, 856, and 1710 nm observed in the PGs are attributed to trigonal bipyramid fivefold coordinated Ni^{2+} [18]. After the thermal treatment, three new bands at 383, 629, and 1060 nm are observed in the GCs, originating from the spin-allowed $^3A_2(F) \rightarrow {}^3T_1(P)$, $^3A_2(F) \rightarrow {}^3T_1(F)$, and $^3A_2(F) \rightarrow {}^3T_2(F)$ transitions of Ni^{2+} in octahedral sites [18]. Our recent comprehensive TEM examination has offered straightforward evidence that nearly all the Ni^{2+} ions are doped into the Ga_2O_3 NCs in the GCs, inducing the pronounced spectral changes, as mentioned above [18]. A ruby-red color

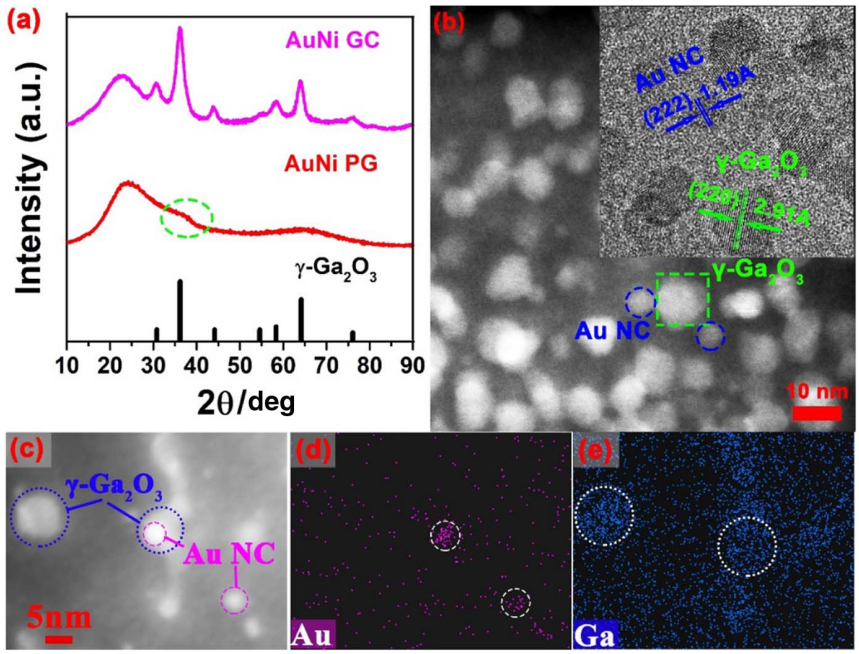

Fig. 1. (a) XRD patterns of the $0.15Ni^{2+}/0.5$Au-codoped PG and GC samples. The pattern of the reference γ-Ga_2O_3 crystal (PDF# 20-0426) is also presented at the bottom. (b) A dark-field TEM image of the GC sample. The inset shows the corresponding HRTEM image, where the blue circles and green squares indicate the presence of Au and Ga_2O_3 NCs, respectively. (c) HAADF-STEM image of the GC sample, and the corresponding STEM-EDS maps for the (d) Au and (e) Ga elements.

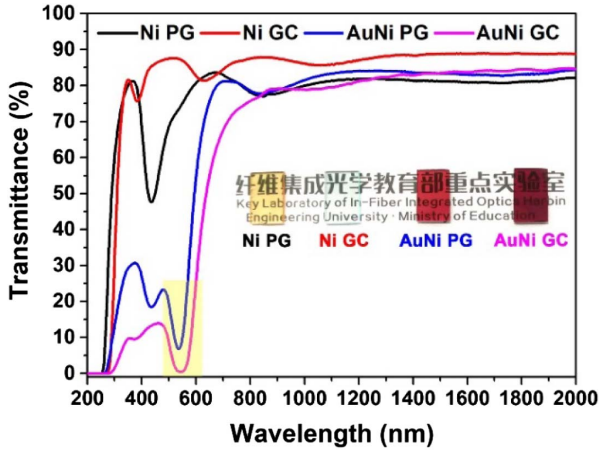

Fig. 2. Transmission spectra of the $0.15Ni^{2+}$ singly-doped and $0.15Ni^{2+}/0.5$Au-codoped PG and GC samples (thickness, 1.2 mm). The inset shows the digital photographs of the samples.

can be seen in the Au-doped PG sample and is slightly darkened in the GC sample due to the increased absorption. This color is caused by LSPR of Au NCs [27]. In a common soda-lime-silicate glass with n of 1.55 close to that of the gallosilicate glass studied herein ($n = 1.57$), the LSPR band peaks at 540 nm for spherical Au-metal NCs of 6 nm in diameter. Remarkably, the LSPR band can be also seen even in the rapidly quenched glass (see Appendix A, Fig. 6), suggesting the spontaneous formation of Au NCs prior to "striking gold" by any thermal treatment [28]. Such a spontaneous formation of Au NCs has been seldom found in glasses, and has only been observed in antimony glasses containing the mild reducing agent of Sb_2O_3 [29].

Both enhancement and attenuation of SPE of RE ions have been found in glasses and GCs embedded with noble metal NCs [30,31]. Herein, when excited at 980 nm, which is off-resonant with respect to the LSPR band of Au-metal NCs (Fig. 2), the SPE of Ni^{2+} centered at 1300 nm with an extremely large FWHM of 283 nm is significantly enhanced by 2 times in the Au/Ga_2O_3 dual-phase GCs as compared with the Ga_2O_3 single-phase GCs [Fig. 3(a)]. The Ni^{2+} emission increases with the Au concentration, reaching the maximum at the 0.5 mol.% Au [Fig. 3(a)]. At higher Au concentrations (>0.5 mol.%), however, some very large Au-metal particles can be seen (by the naked eye), segregating from the samples due to the limited Au solubility. Consequently, the PL intensity starts to fall as the Au-metal NCs embedded in the glass matrix actually decreases after the Au-metal segregation. On the other hand, when excited at 532 nm, which is resonant with the Au LSPR band, the Ni^{2+} SPE is much weaker in the dual-phase than in the single-phase GCs [Fig. 3(b)]. The SPE enhancement is usually accompanied by an increase in the PL decay rate, Γ_r, which is inversely proportional to the lifetime [32]. However, the decay rate of the Ni^{2+} emission decreases in the dual-phase GCs when pumped off-resonantly at 980 nm [Fig. 3(c)] or resonantly at 532 nm with the Au LSPR band [Fig. 3(d)]. Therefore, the decay rate shows a trend opposite to the SPE enhancement.

Below we first address the abnormal behavior of the PL decay rate. Because Ni^{2+} ions are well doped in the Ga_2O_3 NCs,

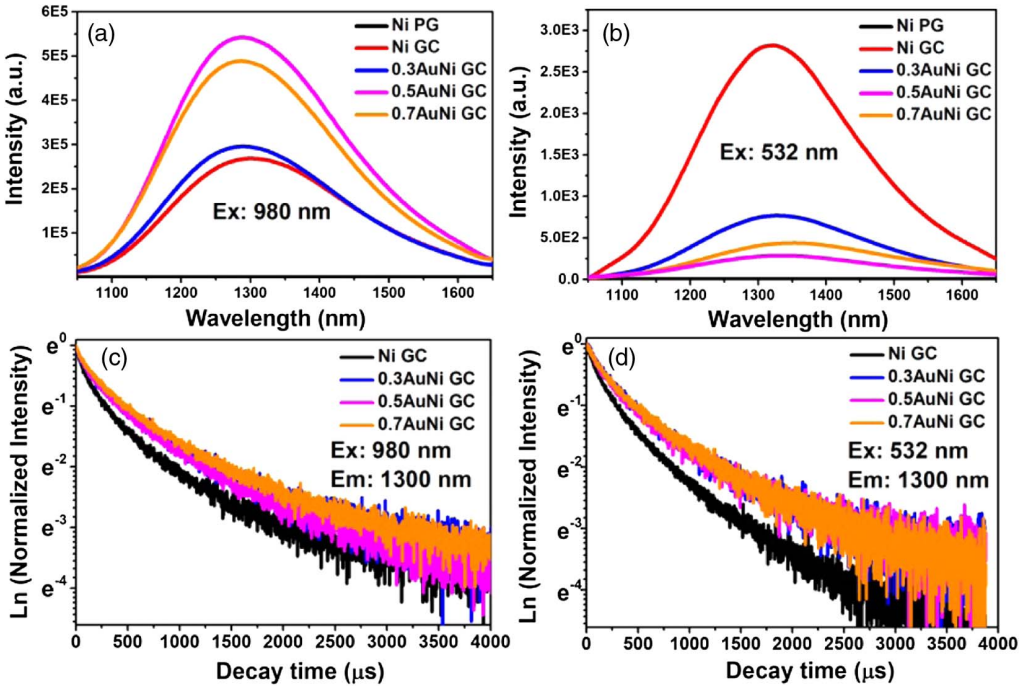

Fig. 3. Emission spectra of the samples doped with 0 mol.% Au (Ni GC), 0.3 mol.% Au (0.3AuNi GC), 0.5 mol.% Au (0.5AuNi GC), and 0.7 mol.% Au (0.7AuNi GC) excited at (a) 980 nm and (b) 532 nm, respectively; PL decay curves of the Ni^{2+} 1300 nm emission of the samples excited at (c) 980 nm and (d) 532 nm, respectively.

their PL decay rate may be described by an "NC cavity" model proposed by Meijerink *et al.* [33], which reads as

$$\Gamma_r = \Gamma_0 n \left(\frac{3n^2}{2n^2 + n_{\mathrm{NC}}^2} \right)^2, \tag{1}$$

where Γ_0 is the PL decay rate of the emitter in vacuum, and n_{NC} is the refractive index of the NC. According to this model, the PL decay rate will increase when NCs are embedded in a matrix with a larger n. The Au-metal NCs slightly increase the effective n of the matrix of the dual-phase GCs to 1.59, and thus the PL decay rate would increase accordingly. Obviously, this is contrary to the experimental observations. The decrease in the PL decay rate could be also caused by reduced nonradiative relaxation. However, Ni^{2+} ions are effectively protected by the Ga_2O_3 NCs with the same crystal field environment. We consider that the decrease in the PL decay rate or, in other words, the increase in the PL lifetime can be attributable to the radiation trapping effect [34] as a result of the emission-reabsorption process, which tends to be enhanced by internal reflection [35]. The dropping of the Ni^{2+} SPE when pumped resonantly at the Au LSPR band is primarily because of the extremely strong and rapid (on the femtosecond scale) energy dissipation (via Joule heating) of the excited Au-metal NCs surpassing any improvement that the field concentration achieves [36].

According to Fermi's golden rule, the radiative transition rate of an emitter from the initial (excited) state $|i\rangle$ to the final state $|f\rangle$ can be described as

$$\Gamma_r = \frac{2\pi}{\hbar} |\langle f | \mu_{if} \cdot E_{\mathrm{loc}} | i \rangle|^2 \rho(\omega), \tag{2}$$

where μ_{if} and E_{loc} are the electric dipole and local electric field operators evaluated at the emitter position, and $\rho(\omega)$ is the LDOS that counts the number of the optical modes available for the emission. The radiative transition rate increases with the LDOS (known as the Purcell effect), which in turn results in the enhanced SPE, given that no additional dissipative channels are introduced [37]. Previously, the SPE enhancement of RE ions (e.g., Eu^{3+}, Er^{3+}) in glasses embedded with Au NCs was interpreted by means of the proliferation of the LDOS near the Au-metal NCs, which becomes most effective when the LSPR band of metal NCs coincides with the optical absorption or emission spectral windows of the emitter. Apparently, this is not the case in the present study, since both the excitation and emission wavelengths of Ni^{2+} are far away from the Au LSPR band. Recently, an enhanced (by 30%) NIR emission of Er^{3+} at 1530 nm was found in a lead germanate glass upon the 980 nm excitation, which is tentatively attributed to the enhancement of optical absorption in the vicinity of hot spots formed near the Au-metal NCs. According to this mechanism, the SPE enhancement (f_F) can be described by the following expression:

$$f_F = \frac{\eta}{\eta_0} \frac{|\mu_{if} \cdot E_{\mathrm{loc}}^{\mathrm{ex}}|^2}{|\mu_{if} \cdot E_0^{\mathrm{ex}}|^2}, \tag{3}$$

where E_0^{ex} and $E_{\mathrm{loc}}^{\mathrm{ex}}$ are the incident and local electric fields at the excitation, and η and η_0 are the quantum efficiencies at the emission in the presence and absence of the Au-metal NCs, respectively. The internal quantum efficiency of Ni^{2+} was determined by $\tau_{300\,\mathrm{K}}/\tau_{10\,\mathrm{K}}$, where $\tau_{300\,\mathrm{K}}$ and $\tau_{10\,\mathrm{K}}$ are the lifetimes of the NIR SPE at RT and 10 K temperatures, respec-

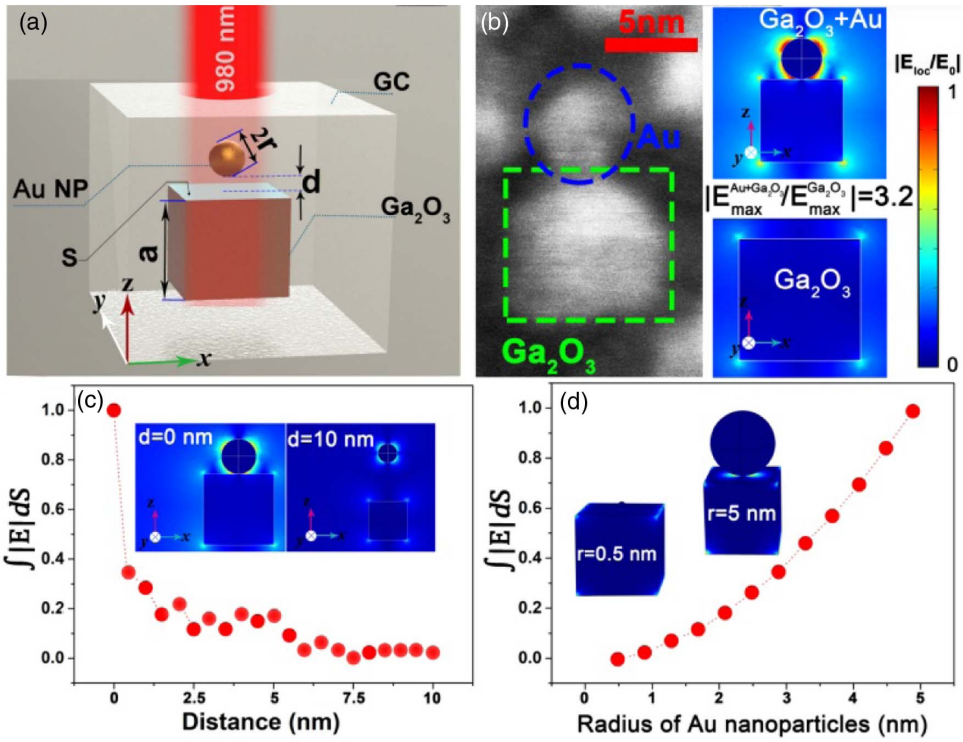

Fig. 4. (a) Simulation model as referred to the TEM image shown in (b); (b) normalized local electric field (E_{loc}) distribution with respect to the incident 980 nm pump light (E_0) in the single-phase Ga_2O_3 (lower right and left) and dual-phase Ga_2O_3 and Au GCs (upper right); normalized integrated local electric field ($\int |E_{loc}| dS$) at the upper surface of the Ga_2O_3 NCs as a function of (c) the distance, d, between Au and Ga_2O_3 NCs and (d) the radius, r, of Au NCs with a fixed distance.

tively. The quantum efficiency is slightly increased from 62% in the absence of Au NCs to 73% otherwise, which accounts for approximately an 18% increase in the SPE. Obviously, the increase in the quantum efficiency cannot be the sole source for the significant increase (>100%) in the SPE of Ni^{2+} in the dual-phase GCs. The enhancement of the local excitation field must also come into play, according to Eq. (3), to account for the enhanced Ni^{2+} SPE. To verify such an assumption, the local field at the pump wavelength due to internal scattering within the GCs was simulated as shown in Fig. 4. The simulation model [Fig. 4(a)] was established according to the sizes and distributions of the Au-metal and γ-Ga_2O_3 NCs determined experimentally by referring to the TEM image [Fig. 4(b)]. The maximum local electric field can be found around the sharp corners of the cubic Ga_2O_3 NCs in the single-phase GCs. The Au-metal NCs clearly act as scattering centers and form a light trapping cage around the Ga_2O_3 NCs. As a result of the light confinement, the strongest electric field can be found to be located between Au-metal and Ga_2O_3 NCs, especially when they are in close proximity (creating a hot spot) [Fig. 4(b)]. The maximum local electric field in the presence of Au-metal NCs is about 3 times larger than that achieved in the single-phase GCs free of Au-metal NCs. Since the local field falls off rapidly with the distance away from the metal NCs [Fig. 4(c)], only a small fraction of Ni^{2+} ions are profiting from the local field enhancement. It is conceivable that, as more Au NCs grow in the glass matrix, the average distance between the Au and Ga_2O_3 NCs becomes shorter, which explains the larger Ni^{2+} SPE enhancement observed in the more strongly Au-doped GC [Fig. 3(a)]. Besides, the simulation also indicates that the local field will increase with the radius of Au-metal NCs [Fig. 4(d)]. Therefore, there is a large chance that further SPE enhancement can be achieved if more Au-metal NCs with larger radii can be planted or grown in the dual-phase GCs. It is also noted that the scattering efficiency is wavelength-dependent [38]. The simulation performed in the Au LSPR band at 532 nm shows that the local field in the dual-phase GCs enhances (by an order of magnitude) to a much greater extent than at the 980 nm (see Appendix A, Fig. 7). However, as most EM wave energy at 532 nm is coupled to heat dissipation of the Au-metal NCs (*vide supra*), only the attenuation of the SPE is observed when pumped at 532 nm [Fig. 3(b)].

Our previous studies have revealed that RE ions tend to be incorporated into the Ga_2O_3 NCs embedded in the single-phase GCs [22]. As a result of the modified local environment, SPE quenching of RE ions is observed. In contrast, enhancements of NIR emissions have been observed from a variety of RE ions (e.g., Yb^{3+}, Er^{3+}) doped Au/Ga_2O_3 dual-phase GCs when pumped off-resonantly (see Appendix A, Figs. 8 and 9). However, when the UCL bands of the RE ions overlap with the strong attenuation band of the Au-metal NCs, or when the RE ions are pumped resonantly with the Au LSPR band, significant PL quenching occurs (see Appendix A, Figs. 10 and 11), which is likely due to the same cause as elaborated above in Fig. 3(b).

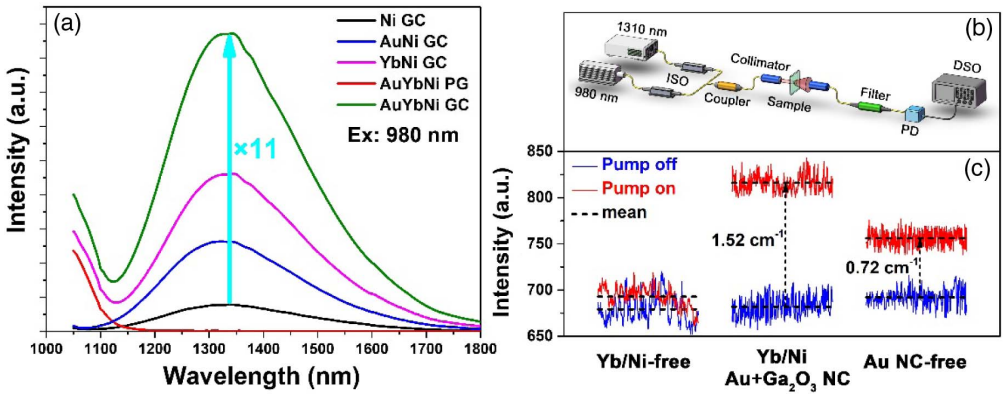

Fig. 5. (a) Emission spectra of the 0.15 mol.% Ni^{2+}-doped single- (Ni GC) and dual-phase (AuNi GC) GC samples, 1.0 mol.% Yb^{3+}/0.15 mol.% Ni^{2+}-codoped single- (YbNi GC) and dual-phase (AuYbNi GC) GC samples excited at 980 nm; (b) scheme of the two-wave mixing method. ISO, isolator; Coupler, at the 980 and 1310 nm wavelengths; Filter, filtering out the 980 nm light; DSO, digital storage oscilloscope; (c) optical amplification properties at 1310 nm of the dual-phase GCs codoped with (in the middle) and without Yb^{3+}/Ni^{2+} (Yb/Ni-free, on the left), and of the single-phase GC codoped with Yb^{3+}/Ni^{2+} (Au NC-free, on the right) for comparison.

Combining the local field enhancement effect of the Au-metal NCs and the sensitization of Yb^{3+} on Ni^{2+}, the Ni^{2+} NIR emission is significantly enhanced over 10 times, which sets a new record-high enhancement factor [Fig. 5(a)]. We further examined the feasibility of the Yb^{3+}/Ni^{2+} (1.0/0.15 mol.%)-codoped dual-phase GCs in optical amplification using the conventional two-wave mixing configuration [39], as schematically shown in Fig. 5(b). The optical gain was evaluated by $g = 1/lLn(I/I_0)$, where l is the sample thickness, and I and I_0 are the signal intensities at 1310 nm with the pump on and off at 980 nm, respectively. The optical gain can be realized both in the dual- and single-phase GCs; however, the presence of Au NCs gives an optical gain (1.52 cm^{-1}) twice that of the Au-free GC sample (0.72 cm^{-1}) [Fig. 5(c)]. The results suggest the potential use of the Yb^{3+}/Ni^{2+}-codoped GCs embedded with dual phase of Au/Ga_2O_3 NCs for optical amplification [40].

We did not measure the light amplification of the sample $x = 0.3$ because of the rather mild enhancement in the PL intensity [Fig. 3(a)]. As for the sample $x = 0.7$, it exhibits significant inhomogeneity, and thus does not warrant further study. It has been previously demonstrated by Qiu *et al.* that fiber can be drawn out of the GC sample similar to the one studied herein by the so-called "melt-in-tube" method [41]. Similar Ni^{2+} SPE was observed from that fiber; however, no light amplification was reported. The light amplification from Ni^{2+}-doped fibers has only been reported by Qiu *et al.* in a GC fiber containing $LiTaO_3$ and $LiAlSi_2O_6$ dual-phase NCs [41]. In contrast to the $LiTaO_3/LiAlSi_2O_6$ dual-phase GCs, which contain anisotropic nonlinear crystals and tend to suffer from birefringence, the Au/Ga_2O_3 dual phase GCs contain only isotropic crystals and thus promise lower scattering losses [42].

4. CONCLUSION

Ni^{2+}-doped GCs containing simultaneously Au-metal/γ-Ga_2O_3-dielectric NCs are fabricated for the first time, to the best of our knowledge. The lengthening of the Ni^{2+} emission lifetime suggests that the NIR SPE enhancement is not related to the increase in the n of the surrounding media and the LDOS at the emission wavelength. Since Ni^{2+} ions are effectively protected by the Ga_2O_3 NCs and consequently kept away from the hydroxyl groups, the reduction of the nonradiative relaxation rate is irrelevant. The significantly enhanced Ni^{2+} SPE in the dual-phase GCs is thus construed by the enhanced local electric field and energy harvesting at the excitation wavelength, because the Au-metal NCs offer more scattering centers with the strongest electric field located between Au-metal and Ga_2O_3 NCs. The enhanced radiation trapping in the dual-phase GCs can account for the lifetime lengthening. The quenching of the SPE when pumped resonantly with the LSPR band of the Au-metal NCs is caused by the rapid energy dissipation of the excited Au-metal NCs. The importance of present study lies in not only providing a promising photonic material for optical amplification, but also in aiding the understanding of the complex mechanisms responsible for the metal NCs enhanced/quenched SPE in optical glasses, which remains highly controversial.

APPENDIX A: EXPERIMENTAL DETAILS

XRD was performed on the powder samples. The diffraction patterns were recorded using an X-ray diffractometer (D/MAX2550VB/PC, Rigaku Corporation, Japan) with Cu-Kα irradiation.

Bright-/dark-field TEM, HRTEM, and HAADF-STEM images were measured using an FEI Talos F200X operating at an acceleration voltage of 200 kV and equipped with an energy-dispersive spectrometer (EDS). TEM samples with a thickness of approximately 50 nm were prepared by ion-beam milling using a PIPS system from GATAN. In the STEM-EDS elemental mapping measurement, the probe size was 0.13 nm in diameter, the examined area (~120 nm × 120 nm) was divided into 2048 pixels × 2048 pixels, and the dwell time was 20 μs per pixel. It took approximately 20 s per frame and 80 s to acquire a mapping image. The selected-area

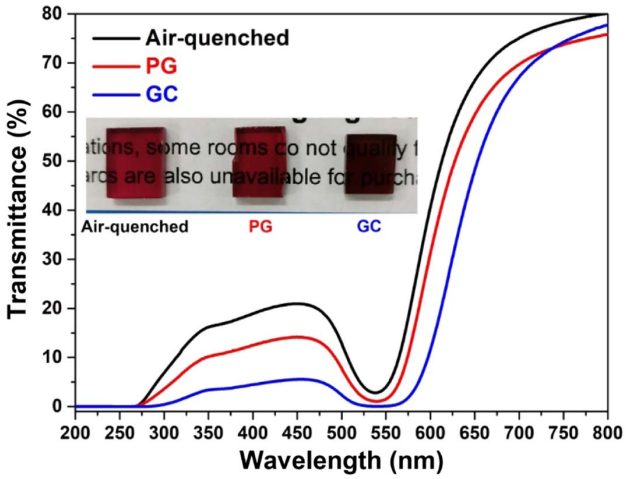

Fig. 6. Transmission spectra of the rapidly quenched (air-quenched) and annealed glasses (PG) and the GC sample doped with 0.5 mol.% Au.

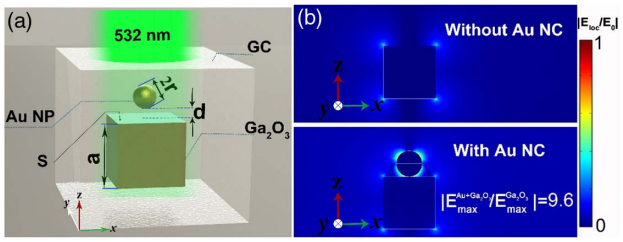

Fig. 7. (a) Simulation model based on the TEM image shown in Fig. 4(b), and (b) local electric field distribution of the light in the Au LSPR band at 532 nm.

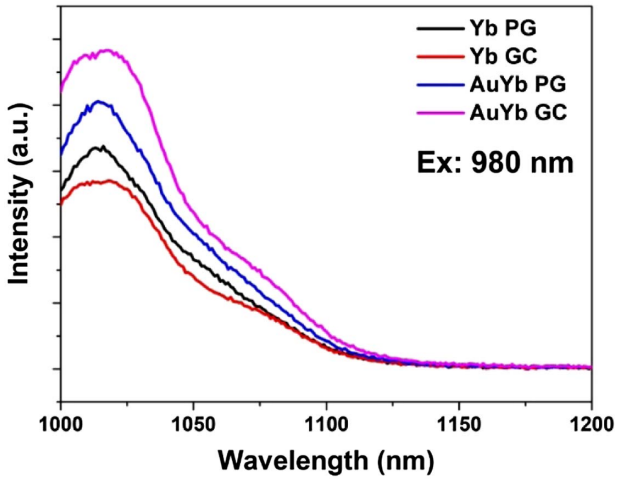

Fig. 8. Emission spectra of the 1.0 mol.% Yb^{3+}-doped (Yb PG) and 1.0 mol.% Yb^{3+}/0.5 mol.% Au-doped (AuYb PG) PGs as well as the 1.0 mol.% Yb^{3+}-doped single- (Yb GC) and dual-phase (AuYb GC) GC samples under 980 nm excitation.

EDS spectrum was obtained by continuously scanning over a 20 nm × 20 nm area. The scanned area was divided into 512 pixels × 512 pixels, and the dwell time was 20 μs per pixel.

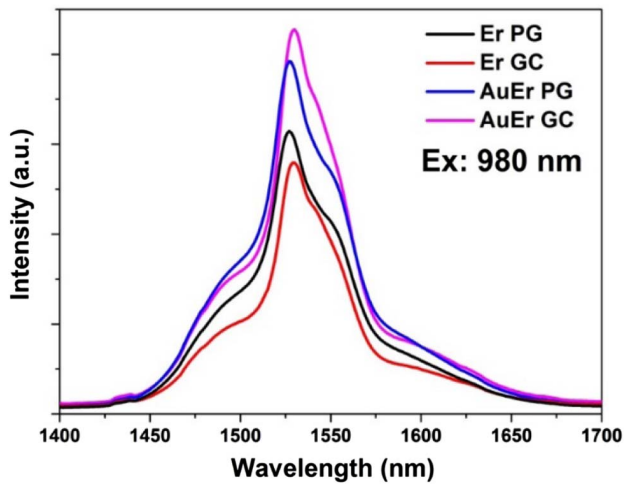

Fig. 9. Emission spectra of the 0.2 mol.% Er^{3+}-doped (Er PG) and 0.2 mol.% Er^{3+}/0.5 mol.% Au-doped (AuEr PG) PGs as well as the 0.2 mol.% Er^{3+}-doped single- (Er GC) and dual-phase (AuEr GC) GC samples under 980 nm excitation.

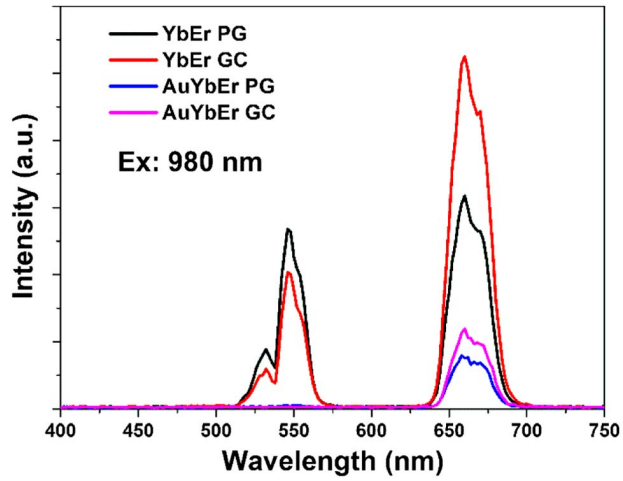

Fig. 10. UCL spectra of the 1.0 mol.% Yb^{3+}/0.2 mol.% Er^{3+}-doped (YbEr PG) and 1.0 mol.% Yb^{3+}/0.2 mol.% Er^{3+}/0.5 mol.% Au-doped (AuYbEr PG) PGs as well as the 1.0 mol.% Yb^{3+}/0.2 mol.% Er^{3+}-doped single- (YbEr GC) and dual-phase (AuYbEr GC) GC samples under 980 nm excitation.

By doing so, the real exposure time was reduced to approximately 0.5 ms, and there was no noticeable damage to the exposed area after the measurements.

Optical transmission spectra were measured using a Perkin-Elmer Lambda 950 UV-VIS spectrophotometer in the spectral range of 200–2000 nm. PL emission and PL decay spectra were recorded using an Edinburgh FLS980 fluorescence spectrometer (Edinburgh Instruments). Continuous- and pulsed-semiconductor lasers, operating at 980 and 532 nm, were used as the excitation sources. The spectral widths of the slits were set to 2 nm. The emission spectra were corrected for the response of a photomultiplier tube (PMT) using a built-in correction file.

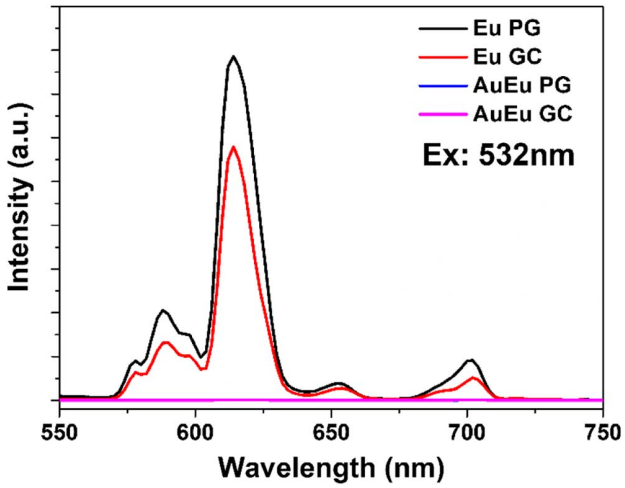

Fig. 11. Emission spectra of the 0.2 mol.% Eu^{3+}-doped (Eu PG) and 0.2 mol.% Eu^{3+}/0.5 mol.%Au-doped (AuEu PG) PGs as well as the 0.2 mol.% Eu^{3+}-doped single- (Eu GC) and dual-phase (AuEu GC) GC samples under 532 nm excitation.

Funding. National Natural Science Foundation of China (11774188, 51872055, 61635007, 61925501); National Key Research and Development Program of China (2016YFF0200704); Natural Science Foundation of Heilongjiang Province (F2017006); Fundamental Research Funds for the Central Universities; Open Fund of the Guangdong Provincial Key Laboratory of Fiber Laser Materials and Applied Techniques (South China University of Technology); PhD Student Research and Innovation Fund of the Fundamental Research Funds for the Central Universities (HEUGIP201819); 111 Project to the Harbin Engineering University (B13015); Incubation Program of Universities' Preponderant Discipline of Shandong Province (03010304).

Acknowledgment. Zhigang Gao and Jing Ren designed the experiments and wrote the draft. Haibo Zhu, Bochao Sun, Yingke Ji, Xiaosong Lu, Hao Tian, and Shu Guo did the measurements. Jianzhong Zhang, Jun Yang, Xiangeng Meng, and Katsuhisa Tanaka discussed the results and commented on the paper. All authors reviewed the paper.

Disclosures. The authors declare no conflicts of interest.

REFERENCES

1. P. Berini and I. D. Leon, "Surface plasmon-polariton amplifiers and lasers," Nat. Photonics **6**, 16–24 (2012).
2. C. Hsu and L. Chou, "Bipolar resistive switching of single gold-in-Ga_2O_3 nanowire," Nano Lett. **12**, 4247–4253 (2012).
3. Y. Ni, C. Kan, L. He, X. Zhu, M. Jiang, and D. Shi, "Alloyed Au-Ag nanorods with desired plasmonic properties and stability in harsh environments," Photon. Res. **7**, 558–565 (2019).
4. G. Lozano, S. R. K. Rodriguez, M. A. Verschuuren, and J. G. Rivas, "Metallic nanostructures for efficient LED lighting," Light Sci. Appl. **5**, e16080 (2016).
5. M. A. Green and S. Pillai, "Harnessing plasmonics for solar cells," Nat. Photonics **6**, 130–132 (2012).
6. M. Pelton, "Modified spontaneous emission in nanophotonic structures," Nat. Photonics **9**, 427–435 (2015).
7. M. P. Busson, B. Rolly, B. Stout, N. Bonod, J. Wenger, and S. Bidault, "Photonic engineering of hybrid metal-organic chromophores," Angew. Chem. Int. Ed. **51**, 11083–11087 (2012).
8. Q. Zhan, X. Zhang, Y. Zhao, J. Liu, and S. He, "Tens of thousands-fold upconversion luminescence enhancement induced by a single gold nanorod," Laser Photon. Rev. **9**, 479–487 (2015).
9. V. Giannini, A. I. F. Domínguez, S. C. Heck, and S. A. Maier, "Plasmonic nanoantennas: fundamentals and their use in controlling the radiative properties of nanoemitters," Chem. Rev. **111**, 3888–3912 (2011).
10. X. Fan, W. Zheng, and D. J. Singh, "Light scattering and surface plasmons on small spherical particles," Light Sci. Appl. **3**, e179 (2014).
11. D. A. Zuev, S. V. Makarov, I. S. Mukhin, V. A. Milichko, S. V. Starikov, I. A. Morozov, I. I. Shishkin, A. E. Krasnok, and P. A. Belov, "Fabrication of hybrid nanostructures via nanoscale laser-induced reshaping for advanced light manipulation," Adv. Mater. **28**, 3087–3093 (2016).
12. X. Xu, W. Zhang, L. Jin, J. Qiu, and S. F. Yu, "Random lasing in Eu^{3+} doped borate glass-ceramic embedded with Ag nanoparticles under direct three-photon excitation," Nanoscale **7**, 16246–16250 (2015).
13. Q. Wang, J. Han, H. Gong, D. Chen, X. Zhao, J. Feng, and J. Ren, "Linear and nonlinear optical properties of Ag nanowire polarizing glass," Adv. Funct. Mater. **16**, 2405–2408 (2006).
14. A. Stalmashonak, A. Abdolvand, and G. Seifert, "Metal-glass nanocomposite for optical storage of information," Appl. Phys. Lett. **99**, 201904 (2011).
15. L. A. H. Fleming, S. Wackerow, A. C. Hourd, W. A. Gillespie, G. Seifert, and A. Abdolvand, "Diffractive optical element embedded in silver doped nanocomposite glass," Opt. Express **20**, 22579–22584 (2012).
16. D. Manzani, D. F. Franco, C. R. M. Afonso, A. C. SantAna, M. Nalin, and S. J. L. Ribeiro, "A new SERS substrate based on niobium lead-pyrophosphate glasses obtained by Ag^{+}/Na^{+} ion exchange," Sens. Actuators B Chem. **277**, 347–352 (2018).
17. V. N. Sigaev, N. V. Golubev, E. S. Ignat'eva, A. Paleari, and R. Lorenzi, "Light-emitting Ga-oxide nanocrystals in glass: a new paradigm for low-cost and robust UV-to-visible solar-blind converters and UV emitters," Nanoscale **6**, 1763–1774 (2014).
18. Z. Gao, S. Guo, X. Lu, J. Orava, T. Wagner, L. Zheng, Y. Liu, S. Sun, F. He, P. Yang, J. Ren, and J. Yang, "Controlling selective doping and energy transfer between transition metal and rare earth ions in nanostructured glassy solids," Adv. Opt. Mater. **6**, 1701407 (2018).
19. Y. Zhang, X. Li, Z. Lai, R. Zhang, E. Lewis, A. I. Azmi, Z. Gao, X. Lu, Y. Chu, Y. Liu, Q. Chai, S. Sun, J. Ren, and J. Zhang, "Largest enhancement of broadband near-infrared emission of Ni^{2+} in transparent nanoglass ceramics: using Nd^{3+} as a sensitizer and Yb^{3+} as an energy-transfer bridge," J. Phys. Chem. C **123**, 10021–10027 (2019).
20. J. Chen, S. Zhou, N. Jiang, S. Lv, and J. Qiu, "Multiscale structured glass for advanced light management," J. Mater. Chem. C **5**, 8091–8096 (2017).
21. Y. Wei, H. E. Heidepriem, and J. Zhao, "Recent advances in hybrid optical materials: integrating nanoparticles within a glass matrix," Adv. Opt. Mater. **7**, 1900702 (2019).
22. Z. Gao, X. Lu, Y. Chu, S. Guo, L. Liu, Y. Liu, S. Sun, J. Ren, and J. Yang, "The distribution of rare earth ions in a γ-Ga_2O_3 nanocrystal-silicate glass composite and its influence on the photoluminescence properties," J. Mater. Chem. C **6**, 2944–2950 (2018).
23. S. Yushanov, J. S. Crompton, and K. C. Koppenhoefer, "Mie scattering of electromagnetic waves," in *Proceedings of the COMSOL Conference* (2013).
24. R. Jurga, F. D. Sala, D. Pisignano, and C. Ciracì, "Enhancement of radiative processes in nanofibers with embedded plasmonic nanoparticles," Opt. Lett. **41**, 1632–1635 (2016).
25. M. Saboktakin, X. Ye, S. J. Oh, S. Hong, A. T. Fafarman, U. K. Chettiar, N. Engheta, C. B. Murray, and C. R. Kagan, "Metal-enhanced upconversion luminescence tunable through metal nanoparticle-nanophosphor separation," ACS Nano **6**, 8758–8766 (2012).
26. H. K. Dan, D. Zhou, R. Wang, Q. Jiao, Z. Yang, Z. Song, X. Yu, and J. Qiu, "Effects of gold nanoparticles on the enhancement of upconversion and near-infrared emission in Er^{3+}/Yb^{3+} co-doped transparent

glass-ceramics containing BaF_2 nanocrystals," Ceram. Int. **41**, 2648–2653 (2015).
27. M. Eichelbaum, K. Rademann, R. Muller, M. Radtke, H. Riesemeier, and W. Gorner, "On the chemistry of gold in silicate glasses: studies on a nonthermally activated growth of gold nanoparticles," Angew. Chem. Int. Ed. **44**, 7905–7909 (2005).
28. F. E. Wagner, S. Haslbeck, L. Stievano, S. Calogero, Q. A. Pankhurst, and K. P. Martinek, "Before striking gold in gold-ruby glass," Nature **407**, 691–692 (2000).
29. T. Som and B. Karmakar, "Enhancement of Er^{3+} upconverted luminescence in Er^{3+}: Au-antimony glass dichroic nanocomposites containing hexagonal Au nanoparticles," J. Opt. Soc. Am. B **26**, B21–B27 (2009).
30. L. R. P. Kassab, D. S. da Silva, R. de Almeida, and C. B. de Araújo, "Photoluminescence enhancement by gold nanoparticles in Eu^{3+} doped GeO_2-Bi_2O_3 glasses," Appl. Phys. Lett. **94**, 101912 (2009).
31. D. M. da Silva, L. R. P. Kassab, A. L. Siarkowski, and C. B. de Araújo, "Influence of gold nanoparticles on the 1.53 μm optical gain in Er^{3+}/Yb^{3+}: PbO-GeO_2 RIB waveguides," Opt. Express **22**, 16424–16430 (2014).
32. Z. Gao, Y. Liu, J. Ren, Z. Fang, X. Lu, E. Lewis, G. Farrell, J. Yang, and P. Wang, "Selective doping of Ni^{2+} in highly transparent glass-ceramics containing nano-spinels $ZnGa_2O_4$ and $Zn_{1+x}Ga_{2-2x}Ge_xO_4$ for broadband near-infrared fiber amplifiers," Sci. Rep. **7**, 1783 (2017).
33. T. Senden, F. T. Rabouw, and A. Meijerink, "Photonic effects on the radiative decay rate and luminescence quantum yield of doped nanocrystals," ACS Nano **9**, 1801–1808 (2015).
34. D. S. Sumida and T. Y. Fan, "Effect of radiation trapping on fluorescence lifetime and emission cross section measurements in solid-state laser media," Opt. Lett. **19**, 1343–1345 (1994).
35. Y. Chu, Q. Hu, Y. Zhang, Z. Gao, Z. Fang, L. Liu, Q. Yan, Y. Liu, S. Sun, G. Peng, E. Lewis, J. Ren, and J. Zhang, "Topological engineering of photoluminescence properties of bismuth- or erbium-doped phosphosilicate glass of arbitrary P_2O_5 to SiO_2 ratio," Adv. Opt. Mater. **6**, 1800024 (2018).
36. J. B. Khurgin, "How to deal with the loss in plasmonics and metamaterials," Nat. Nanotechnol. **10**, 2–6 (2015).
37. M. D. Birowosuto, S. E. Skipetrov, W. L. Vos, and A. P. Mosk, "Observation of spatial fluctuations of the local density of states in random photonic media," Phys. Rev. Lett. **105**, 013904 (2010).
38. P. K. Jain, K. Seok Lee, I. H. El-Sayed, and M. A. El-Sayed, "Calculated absorption and scattering properties of gold nanoparticles of different size, shape, and composition: applications in biological imaging and biomedicine," J. Phys. Chem. B **110**, 7238–7248 (2006).
39. M. M. Martins, L. R. P. Kassab, D. M. da Silva, and C. B. de Araújo, "Tm^{3+} doped Bi_2O_3-GeO_2 glasses with silver nanoparticles for optical amplifiers in the short-wave-infrared-region," J. Alloy. Compd. **772**, 58–63 (2019).
40. Y. Yu, Z. Fang, C. Ma, H. Inoue, G. Yang, S. Zheng, D. Chen, Z. Yang, A. Masuno, J. Orava, S. Zhou, and J. Qiu, "Mesoscale engineering of photonic glass for tunable luminescence," NPG Asia Mater. **8**, e318 (2016).
41. Z. Fang, S. Zheng, W. Peng, H. Zhang, Z. Ma, G. Dong, S. Zhou, D. Chen, and J. Qiu, "Ni^{2+} doped glass ceramic fiber fabricated by melt-in-tube method and successive heat treatment," Opt. Express **23**, 28258–28263 (2015).
42. Z. Gao, Z. Lai, K. Lu, S. Guo, L. Liu, F. He, P. Yang, J. Ren, J. Zhang, and J. Yang, "Efficient green upconversion luminescence in highly crystallized ultratransparent nano-glass ceramics containing isotropic KY_3F_{10} nanocrystals," Opt. Lett. **44**, 4674–4677 (2019).